Impact of zonal flows on turbulent transport in tokamaks

G.L. Falchetto 1)2), Y. Sarazin 1), X. Garbet 1), Ph. Ghendrih 1), M. Ottaviani 1),
S. Benkadda 2), P. Beyer 2)

1) Association Euratom–CEA, CEA/DSM/DRFC Cadarache, France.
2) Laboratoire PIIM, CNRS – Université de Provence, Marseille, France.

e-mail contact of first author: gloria.falchetto@up.univ-mrs.fr

Abstract. Zonal flows (ZFs) are known to play a prominent role in the self-regulation of turbulence in tokamak plasmas. Non-linear fluid numerical simulations of flux-driven turbulence in the core and in the Scrape-Off Layer (SOL) of tokamak plasmas are presented here, which investigate the dependence of zonal flows on plasma and geometric parameters, and their effect on turbulent transport. Core Ion Temperature Gradient (ITG) turbulence is studied with a three-dimensional global model in which zonal flows are damped by ion-ion collisions. Improved confinement is observed as collisionality is decreased at constant injected heat flux. This is found to result from the non-linear upshift of the effective threshold for ITG instability, mediated by an increase of the ZF shear. It is also shown that the threshold for the turbulence onset, and therefore the effective conductivity, increases with input power. The fluctuation characteristics are analyzed in detail and correlation functions are presented. Interchange turbulence is studied in the SOL assuming flute modes. When the so-called sheath conductivity, which governs parallel losses, is small, turbulent transport is controlled by ZFs: its level strongly increases when ZFs are artificially suppressed. At sufficiently larger conductivity ZFs eventually no longer regulate the turbulence. In this case, the sheath response prevents local interactions in wavenumber space to drive ZFs and it clamps the electric potential to the floating potential.

1. Introduction

Large scale flows such as zonal flows (poloidally and toroidally symmetric ExB flows) are known to play a prominent role in regulating the turbulence level in tokamak plasmas [1]. Whereas the generation of zonal flows from turbulence by a parametric or modulational instability mechanism is understood, the dynamics and saturation of such self-generated flows, as well as their dependence on plasma parameters and quantitative impact on turbulent transport, are still a matter of debate. The latter point is crucial to assess transport predictions for ITER. The present paper investigates this question in the core and in the Scrape-Off Layer (SOL) of tokamak plasmas, by means of fluid simulations of flux-driven turbulence [2, 3, 4]. Especially, ion-ion collisionality appears to regulate the zonal flow amplitude in the core, and ultimately the Ion Temperature Gradient (ITG) driven turbulence. In the SOL, sheath boundary conditions are shown to play a crucial role in such a regulation.

Most of the theoretical studies on the scalings of heat turbulent transport ignore the effect of collisionality, on account of the essentially collisionless character of the underlying microturbulence. However, it was first highlighted in [5] that an undamped component of the poloidal flow persists in collisionless plasmas, which is ultimately damped by ion-ion collisions. This drew the attention to a mechanism by which the ion collisionality can affect the overall transport. The role of the undamped zonal flow component on turbulent transport, has been studied theoretically [6] and by direct non-linear numerical simulations [7, 8]. Simulation results are in agreement with the theoretical prediction of a reduction of the zonal flow level and a concomitant increase of transport, as the ion-ion collisionality increases. This mechanism has been

clearly shown in three-dimensional global gyrokinetic particle simulations [8, 9], with fixed pressure gradient boundary conditions.
Compared to the models used in previous numerical studies, fluid simulations with flux boundary conditions present the advantage of allowing the study of the turbulent plasma in reactor steady-state like conditions, on account of the easier accessibility to integration times longer than the energy confinement time. This allowed us to explore the effect of both the collisional damping and of the injected heat flux on core thermal transport *in a turbulent stationary state*, where the equilibrium profiles result from the self-regulation of the flux-driven turbulence and the damped zonal flows. The model and results of the study on the effect of collisionality on core plasma turbulence are presented in Section 2.
The model used for the study of interchange turbulence in the SOL is detailed in Section 3; results are presented on the role of sheath boundary conditions on the regulation of large scale flows.

2. ITG turbulence with collisionally damped zonal flows in the plasma core

A minimal three-dimensional fluid model for electrostatic ITG turbulence is used [4], consisting of the evolution equations of three macroscopic fields: the ion density, the parallel velocity and the ion pressure. Electrons are assumed as adiabatic; use is made of the quasi-neutrality condition and of a simple parallel Landau damping closure. Curvature effects are included as well as a model for the collisional damping of zonal flows. The simulation domain is a toroidal annulus, at the inner boundary of which a constant incoming heat flux is imposed. The normalised model equations are the following :

$$\frac{d}{dt}w - 2\,\varepsilon\,\omega_d\,(\Phi + p_i) + A\nabla_\parallel v + \frac{\kappa_n}{r}\partial_\theta\Phi = -A\,\gamma_{pfd} < w > + D_w\nabla^2 w\,, \tag{1}$$

$$\frac{d}{dt}v + A\nabla_\parallel(\Phi + p_i) - 4\,\varepsilon\,\omega_d\,v = D_v\nabla^2 v\,, \tag{2}$$

$$\frac{d}{dt}p_i + \Gamma A\nabla_\parallel v - 2\Gamma\,\varepsilon\,\omega_d\,(2p_i + < \Phi >) = -\gamma_L|\nabla_\parallel|\,p_i + D_p\nabla^2 p_i\,; \tag{3}$$

where $w = \Phi - < \Phi > -\rho_*^2\nabla^2\Phi$ is the ion guiding center density, Φ the electrostatic potential, $< . >$ represents an average over a magnetic surface; $d/dt = \partial_t + \vec{\mathbf{v}}_E\cdot\nabla$, $\vec{\mathbf{v}}_E = -(\nabla\Phi\times B)/B^2$; $\omega_d = \sin\theta\partial_r + \frac{1}{r}\cos\theta\partial_\theta$ is the curvature operator; $\rho_* = \rho_s/a$ the ion sound Larmor radius normalised to the minor radius, $\varepsilon = a/R$ the inverse aspect ratio, R the major radius, $A = \varepsilon/\rho_*$, $\kappa_n = \nabla n_0/n_0$ and $\Gamma = 5/3$. Lengths are normalised to the minor radius, the parallel velocity to $c_s = \sqrt{T_e/m_i}$, the ion temperature to T_e and the potential to T_e/e; time and conductivity are in Bohm units $t_{Bohm} = a^2/\chi_{Bohm}$, $\chi_{Bohm} = (cT_e/eB)$. The poloidal flow damping is modelled through a damping rate $\gamma_{pfd} = 2/3\;\nu_*\;\varepsilon^{1/2}/q$, which is proportional to the collisionality $\nu_* = \nu_{ii}\;\varepsilon^{-3/2}/(c_s/qR)$ [5], where ν_{ii} is the ion-ion collision frequency and q the safety factor.

The simulations have been performed with the ETAI3D code [10, 4]. As to assess the impact of ion collisions on turbulent transport, simulations have been run for the case of a torus having $\rho_* = 0.02$ and $\rho_* = 0.01$, with fixed injected fluxes $F_{in} = 0.05, 0.2, 0.5$ (measured in units of $\rho_* c_s T_e n_e$) and values of the collisionality varying in the banana regime. A flat density profile and a linear safety factor profile $q = 4r$, are used; $R/a = 4$ and $\gamma_L = 1$. Note that in the simulations presented here the $m = (0, 1)$ coupling in the curvature operators is switched off.

The impact of ion collisions on turbulent transport is a consequence of the self-regulation of drift-waves and zonal flows: at lower collisionality zonal flows are less damped and can be more effective in stabilizing the turbulence, so that ultimately collisions regulate the turbulence. This is highlighted in Fig. 1, where snapshots of the electrostatic potential (b-d) and its fluctuating part (a-c) on a poloidal section, in stationary state, are represented for two different values of the collisionality $\nu_* = 3.5$ (upper plots) and $\nu_* = 0.7$ (lower plots). It is evident how radially extended structures which are present at high collisionality (a) give the place to localised sheared flows when the collisionality is lowered (d).

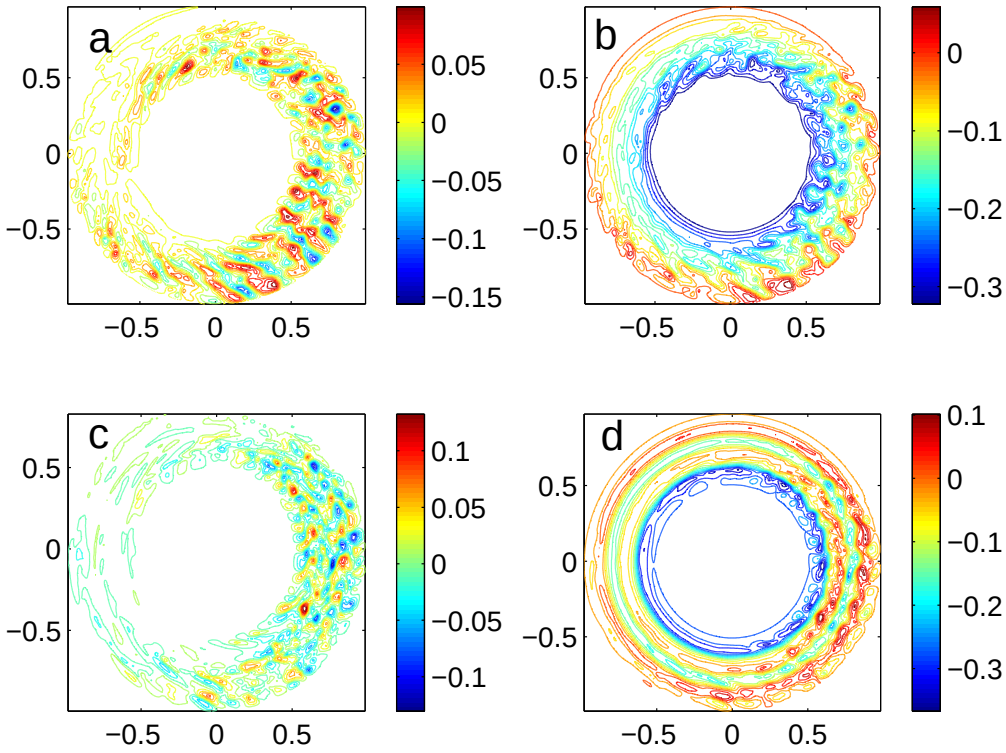

Figure 1: *Contours of the electrostatic potential Φ (b-d) and its fluctuating part $\tilde{\Phi}$ (a-c) on a poloidal section of a tokamak, for two turbulent stationary states corresponding to two different values of collisionality $\nu_* = 3.5$ (upper plots) and $\nu_* = 0.7$ (lower plots), and given injected flux $F_{in} = 0.025$ (in units of $\rho_* c_s T_e n_e$); $\rho_* = 0.01$. The extension of radial convective cells is highlighted in (a-c).*

The net effect is an increase of thermal confinement. Following a sudden reduction of collisionality, one observes that this occurs in two steps, as it was detailed in [4]. First, the fluctuation amplitude decreases, leading to a radial transport reduction. Subsequently, the temperature gradient and the fluctuations rise again until a steady state is reached when the turbulent losses balance the given injected flux. The key mechanism is zonal flow damping: a reduction of collisionality increases the zonal flow shear, a stabilising factor for ITG turbulence, thereby rising the effective ITG threshold. As a consequence, the effective ion heat conductivity increases with collisionality. A similar effect occurs with increased injected power. In this case, the dependence on input power is the result of two opposite effects, the intrinsic degradation due to the increased temperature gradient and the stabilising effect from the increased zonal flow. The temperature gradients in steady-state are shown in Fig. 2, as a function of the collisionality and of the injected fluxes. Note that the average temperature gradient in steady-state does not strongly exceed the effective critical gradient, thus the system is kept fairly close to threshold.

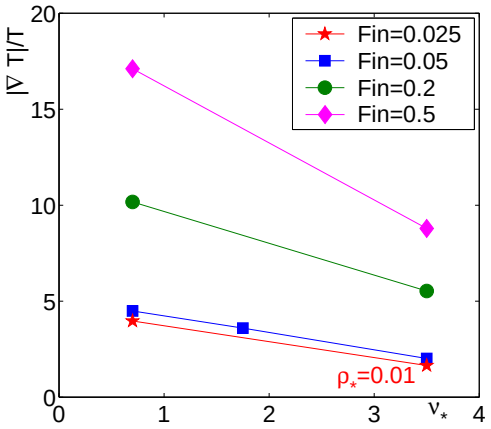

Figure 2: *Steady-state average temperature gradient as a function of the collisionality ν_*, for different injected fluxes and $\rho_* = 0.02$. The data in red line correspond to a case with $\rho_* = 0.01$ and $F_{in} = 0.025$.*

The effect of collisionality on the profiles is shown in Fig. 3, where the self-generated poloidal velocity (left) and the corresponding pressure profiles (right), averaged on a stationary state, are plotted for two values of the collisionality, for the same simulations of Fig. 1. We observe that the stronger zonal flows occurring at lower collisionality appear to be practically *frozen*, since they evolve very slowly, as indicated by the time autocorrelation functions discussed below, and their spatial structure persists for over a confinement time with very little fluctuations; this situation also corresponds to a steepening of the pressure profile.

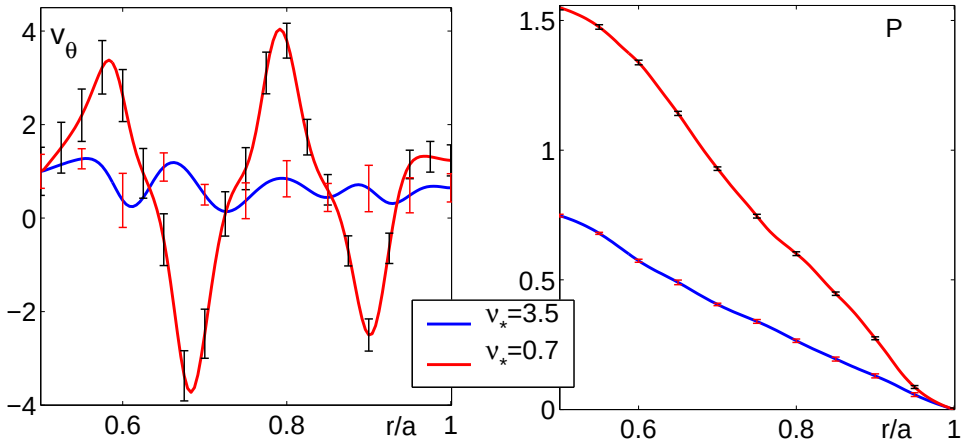

Figure 3: *Self-generated poloidal velocity profile v_θ (left) and corresponding pressure profile (right) averaged on an energy confinement time in stationary state, for a case with $\rho_* = 0.01$, fixed injected flux $F_{in} = 0.025$ and two different values of collisionality ν_*. The vertical bars indicate the amplitude of the variation of the flow around its average.*

Time autocorrelation functions are evaluated for the fluctuating and zonal component of the electrostatic potential for all the simulations in stationary state, averaging over the poloidal and radial coordinates and over several turnover times, typically over two confinement times. A typical case is plotted in Fig. 4, corresponding to a simulation with $\rho_* = 0.02$ and $F_{in} = 0.2$. The first observation is that correlation times strongly depend on the collisionality value. It is also evident, in particular in the low collisionality case, that the turbulence correlation time is an order of magnitude smaller than that of zonal flows, typically $10^{-2} t_{Bohm}$. This clearly shows that the zonal flows evolve much more slowly than the ambient turbulence, supporting the picture of frozen zonal flows discussed above. Note that this can be of practical use for analytic calculations, since it allows to separate the time-scales of turbulence and of zonal flows.

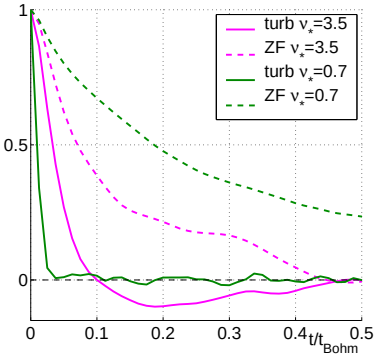

Figure 4: *Time autocorrelation functions for the fluctuating electrostatic potential* $\tilde{\Phi}$ *(full lines) and its zonal component (dashed lines), for two values of the collisionality* ν_* *and* $F_{in} = 0.2$.

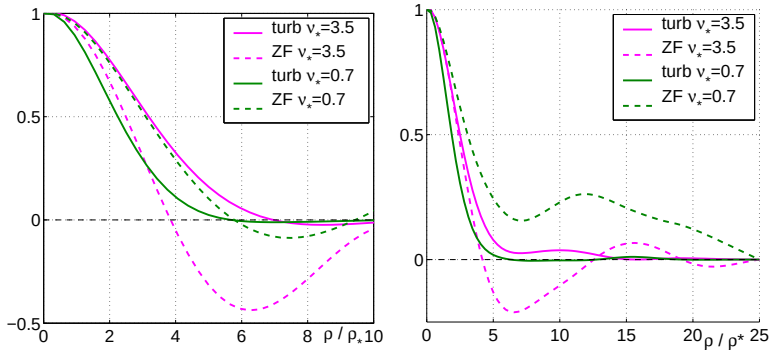

Figure 5: *Two-point radial correlation functions averaged over a confinement time, for the fluctuating electrostatic potential* $\tilde{\Phi}$ *(full lines) and its zonal component* $< \Phi >$*(dashed lines), for two injected fluxes* $F_{in} = 0.005$ *(left plot),* $F_{in} = 0.2$ *(right plot) and two values of the collisionality* ν_*.

Two-point radial correlation functions for the fluctuating electrostatic potential and its zonal component are also evaluated, in the stationary state, averaging over the poloidal coordinate and over a confinement time. The dependence of correlations lengths on both the collisionality and the injected flux can be observed in Figs. 5, where correlation functions are shown for two values of collisionality and injected fluxes $F_{in} = 0.05$ (left plot), $F_{in} = 0.2$ (right plot).
One can observe that the turbulence correlation lengths slightly decrease with decreasing collisionality, growing with ν_*/F_{in}, whereas the zonal flow correlation lengths show an inverse dependence. However, the radial correlation lengths of the turbulence and of the zonal flows, evaluated as the half-height width, are comparable. Correlation functions for the fluctuating component decay exponentially and do not present significant tails at large radial separation, whereas it is interesting to note that the zonal flow component shows an oscillation of several Larmor radii of amplitude.
The radial correlation functions are observed to be self-similar for different tokamak sizes, as shown in Fig. 6 for two simulations having respectively $\rho_* = 0.02, F_{in} = 0.005$ and $\rho_* = 0.01, F_{in} = 0.025$ ($\nu_* = 3.5$). The typical radial size of turbulent structures results to be of the order of $3.3 \pm 0.1\rho_*$.

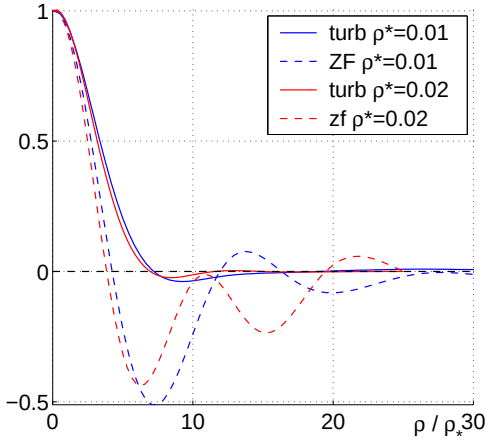

Figure 6: *Two-point radial correlation functions averaged over a confinement time, for the fluctuating electrostatic potential* $\tilde{\Phi}$ *(full lines) and its zonal component* $< \Phi >$ *(dashed lines), for two self-similar simulations at* $\nu_* = 3.5$ *having respectively* $\rho_* = 0.02, F_{in} = 0.005$ *(red) and* $\rho_* = 0.01, F_{in} = 0.025$ *(blue).*

3. Large-scale flows in SOL interchange turbulence

Interchange turbulence [11] is studied in the SOL with a fluid model. Several approximations are made. The electron temperature T_e is taken constant, and a cold ion limit $T_i/T_e \ll 1$ is considered. Assuming flute modes allows for a field line average, which makes the system two dimensional. Particle balance and charge conservation then couple the total density n and the electric potential ϕ:

$$\partial_t n + [\phi, n] = S - \sigma_{||}\, n\, \mathrm{e}^{\Lambda-\phi} + D\nabla_\perp^2 n \tag{4}$$

$$\partial_t \nabla_\perp^2 \phi + [\phi, \nabla_\perp^2 \phi] = \sigma_{||} \left\{1 - \mathrm{e}^{\Lambda-\phi}\right\} - g\, \partial_y \log(n) + \nu\nabla_\perp^4 \phi \tag{5}$$

Distances are normalized to the Larmor radius $\rho_s = m_i c_s/eB$ and time to $\omega_c^{-1} = m_i/eB$. The Poisson brackets derives from the $E \times B$ advection: $[\phi, h] \equiv \partial_x\phi\partial_y h - \partial_y\phi\partial_x h$, with x and y the radial and diamagnetic coordinates, respectively. This model captures some essential features of the interchange instability. First, it is flux-driven, in the sense that a constant particle source S, radially localized, drives the system out of equilibrium. Then, the average field line curvature $g \propto \rho_s/R$ accounts for both favorable and unfavorable regions. Finally, the sheath Bohm criterion is accounted for through the parallel boundary conditions: parallel losses are proportional to the sheath conductivity $\sigma_{||} = \rho_s/L_{||}$. $\Lambda \approx \log(m_i/m_e)$ is the floating potential. Most of the dynamical properties of the system are discussed in references [3, 12]. The present paper emphasizes the impact of $\sigma_{||}$ on the large-scale flows, and ultimately on the turbulent transport. These flows correspond to the $k_y = 0$ component of the velocity along y, namely $v_y = \partial_x\phi$, and are reminiscent of ZFs in the core plasma. From eq.5, the dynamics of $\langle v_y \rangle$ is governed by:

$$\partial_t \langle v_y \rangle = -\partial_x \langle \tilde{v}_x \tilde{v}_y \rangle + \sigma_{||} \int_0^x \langle 1 - \exp(\Lambda - \phi) \rangle dx + \nu \partial_{xx} \langle v_y \rangle \tag{6}$$

The Reynolds stress dominates by about one order of magnitude over the sheath term. The viscosity ν controls the linear damping of $\langle v_y \rangle$.

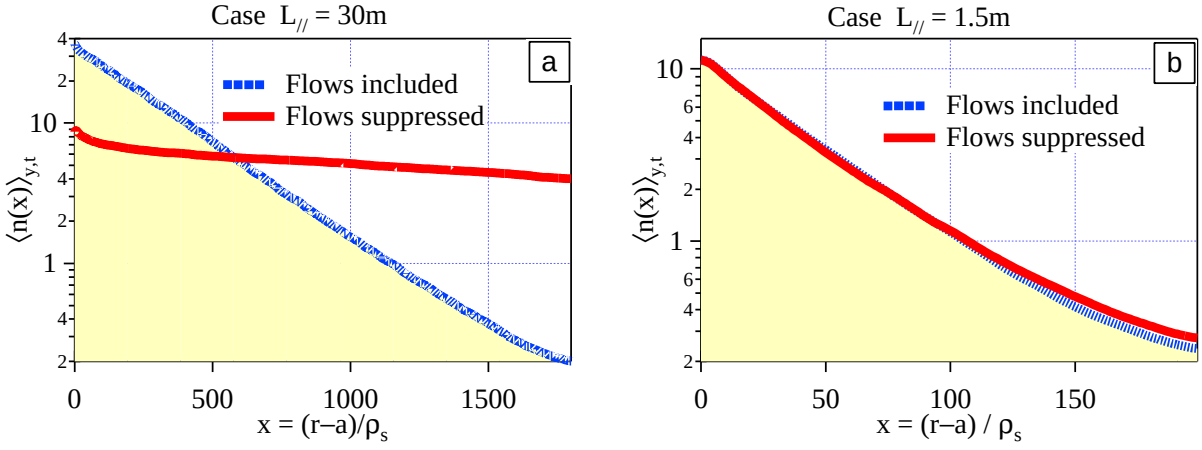

Figure 7: *Mean density profiles for a small (a) and a large (b) value of $\sigma_{||}$, when large-scale flows are included or not.*

So as to assess the impact of the large-scale flows on the transport, a set of four simulations has been performed: with and without these flows for two different values of $\sigma_{||}$, corresponding to long ($L_{||} = 30\mathrm{m} \rightarrow \sigma_{||} \approx 1.13\,10^{-5}$) or short ($L_{||} = 1.5\mathrm{m} \rightarrow \sigma_{||} \approx 2.27\,10^{-4}$) parallel

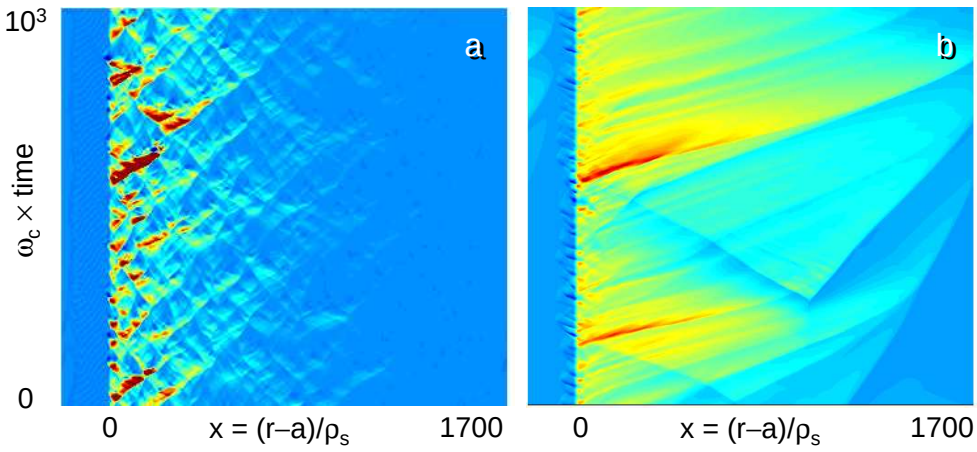

Figure 8: *Dynamics of the radial particle flux* Γ *for* $L_{\parallel} = 30$ *when fbws are included (a) or not (b).*

connection lengths in the SOL. The simulations without fbws are carried out with $\langle v_y \rangle$ set artificially to zero. Since the SOL e-folding length λ_n increases with $L_{\parallel}$, runs at low $\sigma_{\parallel}$ require a large radial box. Indeed, a simple estimate based on a diffusive turbulent transport yields $\lambda_n \propto L_{\parallel}^{1/2}$.

The results are the following. For small $\sigma_{\parallel}$, the inclusion of fbws in the model generates a strong reduction of the particle transport, typically by one order of magnitude, as highlighted by the mean density profiles $\langle n \rangle$ (Fig.7a). A drastic change in the transport dynamics is also observed, with more frequent and smaller avalanches. Also, the effective velocity of the propagating fronts is much reduced, typically by a factor of four, as exemplified on Fig.8. The relative magnitude of density fluctuations $\delta n / \langle n \rangle$ is however similar in both cases, of order of 10%. In such a regime, a good correlation is observed between the zonal fbw activity and the broadening of the radial spectrum of ϕ. This is consistent with the random shearing of turbulent eddies by zonal fbws, which leads to an increase of the mean square radial wave number, as suggested in reference [13]. Conversely, at sufficiently large $\sigma_{\parallel}$, the zonal fbw amplitude decreases significantly, such that zonal fbws eventually no longer regulate the turbulence (Fig.7b).

These observations are found to result from the specific non linear response of the sheath boundary. First, the linear analysis of eqs.4-5 reveals that large y-structures, $i.e.$ those with vanishing

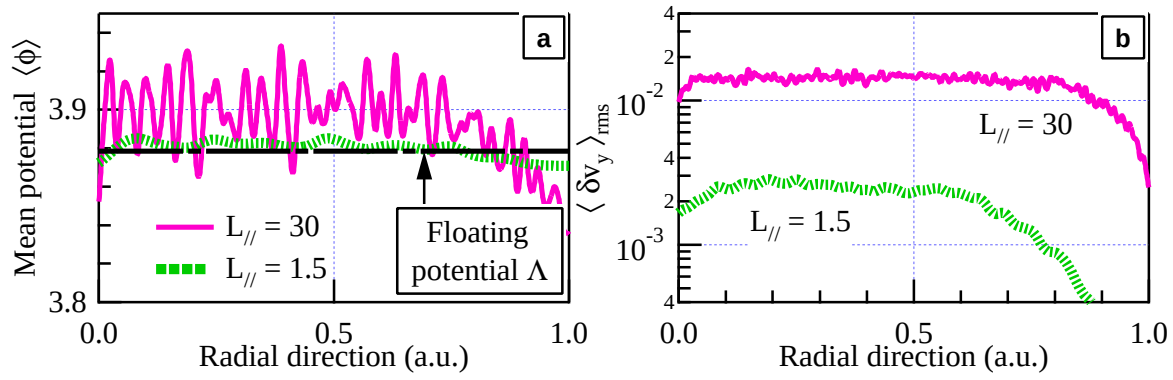

Figure 9: *Mean profi les of the electric potential (a) and of the root mean square of the large-scale fbw fluctuations (b) for* $L_{\parallel} = \{1.5, 30\}$.

k_y, are damped by $\sigma_\parallel$. Consequently, large values of $\sigma_\parallel$ make local interactions in wavenumber space inefficient at low k_y, thus inhibiting the zonal flow build-up from the small wavenumbers. Secondly, at large $\sigma_\parallel$, the electric potential ϕ is clamped to the floating potential Λ. Indeed, the balance between transverse and parallel currents in eq.5 imposes: $\phi \approx \Lambda + (gk_y/\sigma_\parallel)\delta n/\langle n \rangle$. In this case, ϕ is almost constant radially and equal to Λ (Fig.9a), leading to a much reduced component of zonal flows (Fig.9b).

4. Conclusions

Fluid simulations of flux-driven drift wave turbulence in the core and in the SOL of a tokamak plasma have been presented. Results from 3D core ITG turbulence show that ion-ion collisions are efficient in regulating ion heat transport. The key element is the increase of zonal flow shear at lower collisionality which rises the effective ITG threshold. The resulting ion heat conductivity is thus reduced at lower collisionality. Measuring the turbulence characteristics, one observes that the main effect of the increased zonal flow shear is a reduction of the turbulence correlation time, whereas the radial correlation length is comparatively less affected. In the SOL, the parallel transport towards plasma facing components appears to be able to reduce the magnitude of zonal flows. Ultimately, the level of turbulent transport and that of zonal flows can be decoupled.

Acknowledgements. The authors would like to acknowledge fruitful discussions on some of these results during the last "Festival de Théorie", held in Aix-en-Provence, France, in July 2003.

References

[1] DIAMOND, P. H., et al., "Review of Zonal Flows" submitted to Plasma Phys. and Control. Fusion (2004).

[2] GARBET, X., WALTZ, R., Phys. Plasmas **5** (1998) 2836.

[3] SARAZIN, Y., GHENDRIH, PH., Phys. Plasmas **5** (1998) 4214.

[4] FALCHETTO, G.L., OTTAVIANI, M., Phys. Rev. Lett. **92(2)** (2004) 25002.

[5] ROSENBLUTH, M. N., HINTON, F. L., Phys. Rev. Lett. **80** (1998) 724.

[6] HINTON, F. L., ROSENBLUTH, M. N., Plasma Phys. Controlled Fusion **41** (1999) A653.

[7] BEER, M. A., HAMMETT, G.W., Phys. Plasmas **3** (1996) 4046.

[8] LIN, Z., et al., Phys. Rev. Lett. **83** (1999) 3645 .

[9] LIN, Z., et al., Phys. Plasmas **7** (2000) 1857.

[10] OTTAVIANI, M., MANFREDI, G., Nucl. Fusion **41** (2001) 637.

[11] NEDOSPASOV, A.V., Sov. J. Plasma Phys. **15** (1989) 659; GARBET, X., et al., Nucl. Fusion **31** (1991) 967.

[12] SARAZIN, Y., et al., J. Nucl. Materials **313-316** (2003) 796; GHENDRIH, PH., et al., Nucl. Fusion **43** (2003) 1013; FIGARELLA, et al., to appear in J. Nucl. Materials (2004).

[13] DIAMOND, P. H., et al., *Proc. 17th IAEA Fusion Energy Conference, Yokohama (1998)*, IAEA-CN-69/TH3/1, IAEA, Vienna (1998).